TU Delft

Delft University of Technology

Microstructural properties and surface roughness of 3D printed open cell-foam

Shikh Anuar, Fadhilah; Mustapha, Khairul Azhar; Sa'at, Fatimah Al Zahrah Mohd; Zini, Nurul Hilwa Mohd; Tokit, Ernie Mat; Narasimmanaidu, Satishwara Rao; Hooman, Kamel

Publication date
2023

Document Version
Final published version

Published in
Jurnal Tribologi

Citation (APA)
Shikh Anuar, F., Mustapha, K. A., Sa'at, F. A. Z. M., Zini, N. H. M., Tokit, E. M., Narasimmanaidu, S. R., & Hooman, K. (2023). Microstructural properties and surface roughness of 3D printed open cell-foam. *Jurnal Tribologi*, *36*, 16-31.

Important note
To cite this publication, please use the final published version (if applicable).
Please check the document version above.

Copyright
Other than for strictly personal use, it is not permitted to download, forward or distribute the text or part of it, without the consent of the author(s) and/or copyright holder(s), unless the work is under an open content license such as Creative Commons.

Takedown policy
Please contact us and provide details if you believe this document breaches copyrights.
We will remove access to the work immediately and investigate your claim.

This work is downloaded from Delft University of Technology.
For technical reasons the number of authors shown on this cover page is limited to a maximum of 10.

Jurnal Tribologi 36 (2023) 16-31

MYTRIBOS Malaysian Tribology Society

Jurnal Tribologi

Website : jurnaltribologi.mytribos.org e-issn: 2289-7232

Microstructural properties and surface roughness of 3D printed open cell-foam

Fadhilah Shikh Anuar [1*], Khairul Azhar Mustapha [1], Fatimah Al-Zahrah Mohd Sa'at [2], Nurul Hilwa Mohd Zini [2], Ernie Mat Tokit [2], Satishwara Rao Narasimmanaidu [2], Kamel Hooman [3]

[1] Fakulti Teknologi Kejuruteraan Mekanikal dan Pembuatan, Universiti Teknikal Malaysia Melaka, Hang Tuah Jaya, 76100, Durian Tunggal, Melaka, MALAYSIA.
[2] Fakulti Kejuruteraan Mekanikal, Universiti Teknikal Malaysia Melaka, Hang Tuah Jaya, 76100, Durian Tunggal, Melaka, MALAYSIA.
[3] Process and Energy Department, Delft University of Technology, Leeghwaterstraat 39, 2628 CB Delft, THE NETHERLANDS.
*Corresponding author: fadhilah@utem.edu.my

KEYWORDS

3D printing
Porous
Surface topology
Pressure drop

ABSTRACT

In this study, the microstructure of open-cell metal foam was generated and reconstructed, to produce a new generation of open-cell foam, which is called 3D printed open-cell foam. At the current stage of research, nylon powder and plastic acid are utilized as the materials for two different 3D printing technologies: Selective Laser Sintering (SLS) and Fused Deposition Modelling (FDM), respectively. The microstructural properties and surface roughness of the 3D printed open-cell foam are investigated using CAD files and microscope images. The surface smoothness and structure strength are found to be dependent on the printing technologies, material employed, and foam size. However, the SLS technology produced smoother ligament surfaces with fewer residues than using the FDM. The ligaments of the small-size 3D printed open-cell foam at the exact size of the metallic foam, on the other hand, are weak and easily shattered. This study also found that the trends of pressure drop from additive manufacturing methods agreed to the original metallic open-cell foam, which are decreasing with the increase of pore sizes.

Received 23 April 2022; received in revised form 7 June 2022; accepted 24 September 2022.
To cite this article: Shikh Anuar et al. (2023). Microstructural properties and surface roughness of 3D printed open cell-foam. Jurnal Tribologi 36, pp.16-31.

1.0 INTRODUCTION

An open-cell metal foam is a metallic material with a structure made of a solid matrix and interconnected pores that has attracted the attention of many researchers over these years. Due to its porous microstructure, one would intuitively know it is promising for wide applications due to its advantageous properties such as lightweight, large specific surface area, and provide excellent fluid mixing as the structure offers torturous flow paths (Alvandifar et al., 2018; Orihuela et al., 2018). In addition, the thermal conductivity of the metal foams can be varied, depending on the used materials and the purpose of the applications, for example, heat exchangers (Rabbani et al., 2019). Meanwhile, to be used as a sound absorber (Liang et al., 2018), the porosity and pore sizes are key factors that need to be considered as compared to the used materials. For fluid-flow applications, the porous structure of open-cell foam may also induce massive pressure drop effects (Ahmed et al., 2019; Alvandifar et al., 2018; Orihuela et al., 2018), which hindered the process of its implementation in the industries. Thus, a partially filled design; where only a part of the flow passage is filled with the open-cell foam was proposed to overcome the pressure drop issue. However, the presence of secondary flow at the interface between clear and porous regions influenced the pressure drop values (Shikh Anuar, Ashtiani Abdi, & Hooman, 2018a). Moreover, the study also found no-flow regions within the porous structure of the partially filled design. Thus, it is skeptical to use a consistent range of pore sizes in the whole one open-cell foam sample, where the pore sizes should be altered to suit certain applications. However, conventional production methods could not produce the variation in the pore sizes in one sample. Regardless of the debated issues, the characteristics of metal foam are being studied in various areas (fluid flow across the structure, heat transfer, absorption, and others), whether by simulation or experimental methods.

For over the years, the only practical methods to manufacture metal foams are by the conventional production methods such as foaming of melts by gas injection and solid-gas eutectic solidification (Banhart, 2000). The production methods required various processes, which are complicated and time-consuming. The possibility of modifying its porous structure for an optimum fluid flow without no-flow regions is also needed to favor the partially filled design with the lower pressure drop effects. A reverse engineering method using Computed Tomography (CT) scans could be used to duplicate the design of a porous metal foam (Matheson et al., 2017). The method involves the analysis of structure images of the porous foam from the translated X-ray beam and then generating the geometry of porous foam, including the pore and ligament diameters. However, a variation in the final output in terms of qualities, physical appearance, and surface roughness should be expected from a variety of additive manufacturing technologies in the market such as selective laser melting, fused deposition modeling, and electron-beam melting (Adekanye et al., 2017). The quality of the printed products depends on the layer thickness, nozzle temperature, platform temperature, printing speed, extruding rate, and layer height in the 3D printing process (Kumaresan et al., 2021). By varying infill patterns, these methods also would influence the maximum energy absorbed and impact strength of the printed samples (Kottasamy et al., 2021).

In practical application, the surface roughness parameter is a major factor that significantly would influence pressure drop, and fluid flow (Li et al., 2021; Pereira et al., 2019; Rocha et al., 2020). The surface roughness may cause a disturbance that affects the flow characteristics such as Reynold number and velocity profile (Ibrahim et al., 2004). In this study, a new generation of open-cell foam is proposed for additional experimental exploration (acoustic, fluid flow, insulator, etc.) in future research work as a replacement to the existing open-cell metal foam in the market.

At this preliminary stage of research, two different 3D printing technologies and materials are used to produce the 3D printed open-cell foams. The surface roughness of the samples is examined using open-source software and microscope images. The pressure drops of the 3D printed open-cell foams with various pore and foam sizes are also investigated experimentally to increase the databank of this new generation of open-cell foam.

2.0 EXPERIMENTAL PROCEDURE

2.1 Reconstruction of Foam Porous Structure

The production of 3D printed open-cell foams included several steps, starting from scanning its porous structure, reconstructing the internal region, and manufacturing the samples using two different 3D printers. The 3D models could be reconstructed using any kind of CAD software such as Blender, AutoCAD, or SOLIDWORKS. However, the attempt of this study to directly convert the DWG file from AutoCAD into STL format was failed. The exact cause is unknown but most probably due to complicated structure of the model itself that consists of a lot of meshes on its ligament surfaces. These meshes are from the original CT-scan images. As an alternative, the SOLIDWORKS has been used, which had successfully converted the file into 3D printing format. Thus, restructuring the CT-scan image is suggested to be done with SOLIDWORKS at the first hand to reduce steps in producing the 3D models. The external geometries and sizes of those 3D printed foams are considered to suit the in-house wind tunnel's test section, which is 0.1m (height) x 0.095m (length) x 0.1m (width). The original real structure of an open-cell metal foam (5 PPI) in Figure 1 (Shikh Anuar, Ashtiani Abdi, Odabaee, et al., 2018b) is enlarged to a scale of 2, 4, 6, and 8 from its original size. Meanwhile, the example of porous open-cell foam CAD drawings could be seen in Figure 2.

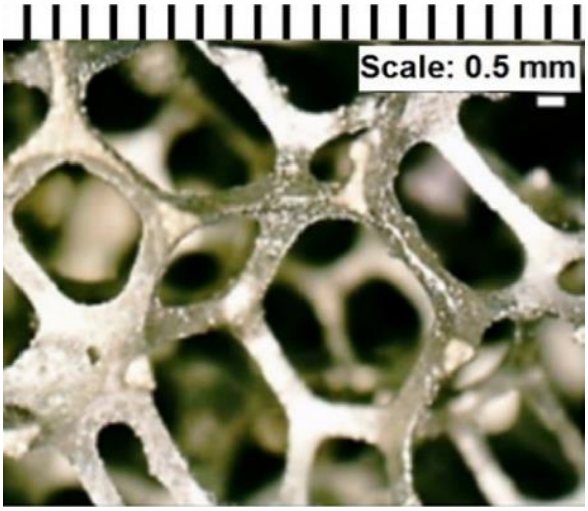

Figure 1: Porous structure of 5 PPI metal foam (Shikh Anuar, Ashtiani Abdi, Odabaee, et al., 2018b).

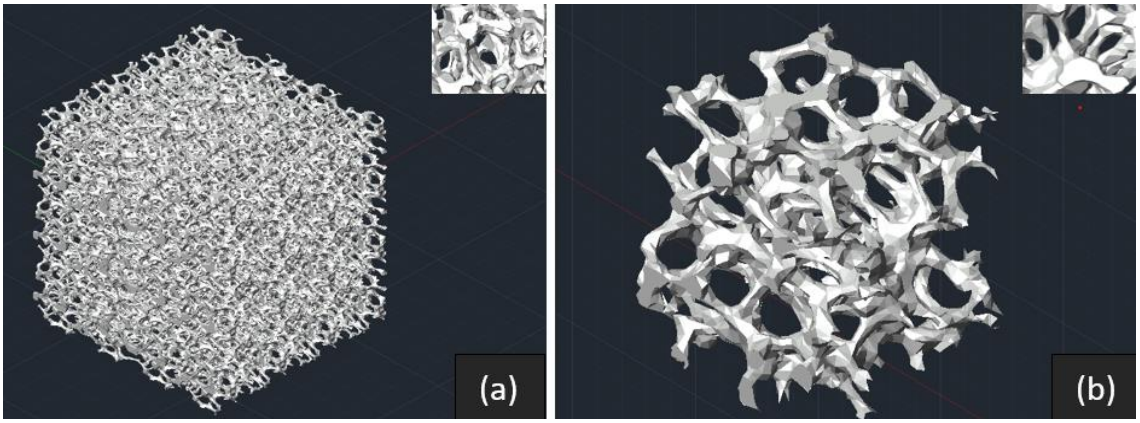

Figure 2: Isometric CAD drawing; (a) 2x upscale, and (b) 8x upscale.

In this study, the 3D-printed open-cell foams are produced using two types of 3D printing technologies; (1) Fused Deposition Modeling (FDM); FlashForge Creator Pro and Selective Laser Sintering (SLS); Farsoon (SS402P model). The FDM is widely used nowadays as it is a cheaper solution than SLS, meanwhile the SLS is the most popular methods for complex designs. Thus, these two 3D printing technologies were used to understand its feasibility in producing the foam models. Both FDM and SLS are some examples of additive manufacturing method for reverse engineering method, where the model is designed through computer aided design (CAD) software and then saved in stereolithography (STL) file format before the process been proceed for manufacturing process (Norani et al., 2021).The FDM or the other name, Fused filament fabrication (FFF) is a manufacturing method via extrusion (Norani et al., 2020, 2021) where it works by ejecting melted filament layer-by-layer onto the forming stage. The printer's nozzle moves along according to the sample structure and shape until the layering is completed and finished (Sachlos et al., 2003). Supports (external structures) are also installed in between the structure to maintain the form and shape of the porous structure while support overhanging or unconnected features (Sachlos et al., 2003). For SLS technology, a raw material in powder form is dispersed in a very thin layer on a platform (a bed of powder) and preheated beneath the powder liquefying point (Walker et al., 2014). The laser sintering on the powdered material took place and bond the material together to create a solid structure. Meanwhile, the unfused powder became support for the product during the printing process. The SLS process has also been through layer-by-layer where the platform moves down to form a new layer of powder on the top and the sintering process is continuous until the part is completed (Herdering et al., 2019). The printed foam models and material properties are shown in Figure 3 and Table 1, respectively.

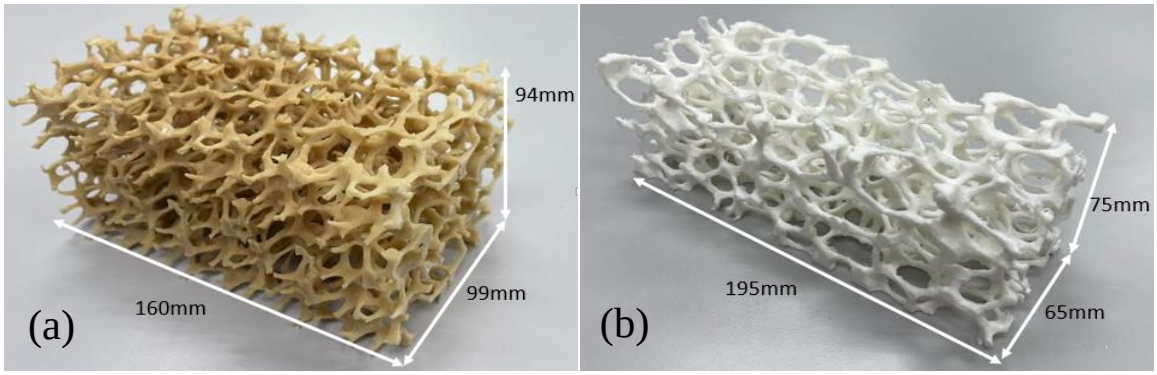

Figure 3: Example of 3D printed open-cell foams produced using different printing technologies, (a) SLS and (b) FDM.

Table 1: Properties of 3D printing materials.

Materials	**Melting Point (°C)**	**Tensile Strength (MPa)**	**Elongation at break (%)**	**Reference**
Polylactic Acid (PLA) – FDM	200 - 240	59	7	(Farah et al., 2016)
FS 3300 PA (nylon) – SLS	183	46	36	(Khudiakova et al., 2020)

2.2 Microstructural Properties and Surface Topology

To classify the 3D printed open-cell foam properties, it has been either been measured or calculated using the existing equation from the literature. For example, the pore size, $d_{p,}$ and ligament diameter, d_l can be directly measured using the microscope and CAD images, while the porosity, ε of the samples is determined using Eq. (1)(Shikh Anuar et al., 2018a). Note that, *m* and ρ in the equation are the mass and density of the foam samples, respectively and V_{total} is the volume of the foam (including the void/pore).

$$= 1 - \frac{m_{solid}/\rho_{solid}}{V_{total}} \quad (1)$$

Table 2 shows the properties of 3D printed open-cell foam and a metallic open-cell foam (China Beihai Building Material) as the benchmarking to the new generation of open-cell foam. Since the original size of metallic foam could not be produced using current 3D printing technologies, only the properties of 4, 6, and 8 scale factors are presented in the table.

The porous structure and ligaments are examined using a RS Pro USB Wi-Fi microscope with (1280 × 1024 pixels, and up to 200× magnification) and the surface roughness is evaluated by an open-source software; Image J in terms of profile plot (gray value against distance, pixels). The gray value is the value of each pixel that represents an amount of light. Thus, the software can be used as a gauge for generalization in comparing two or more different samples. By subtracting the

background of the sample images, the surface roughness is determined thoroughly. The examples of the sample images are shown in Figure 4. Note that the lines on the surface came in Figure 4 (c) and (d) are from the layering effect from FDM. The images are set up at 32 bits for post-processing. In this case, the images of foam (ligament) surfaces are extracted from the foam samples with 6 and 8 scale factors for a larger flat surface area to ease the image processing.

Table 2: Comparison of physical properties between 3D printed foam (SLS) and metallic foam

Foam physical properties	**3D printed open-cell foam**				**Metallic open-cell foam (Shikh Anuar, Ashtiani Abdi, Odabaee, et al., 2018b)**
Pore density (PPI)/ Scale	2 scale	4 scale	6 scale	8 scale	10 PPI
Ligament diameter, dl (m)	0.00093	0.00198	0.00275	0.00380	0.00044
Pore diameter, dp (m)	0.00839	0.01003	0.01525	0.02305	0.00256
Porosity, ε (–)	0.87	0.87	0.89	0.90	0.82-0.91

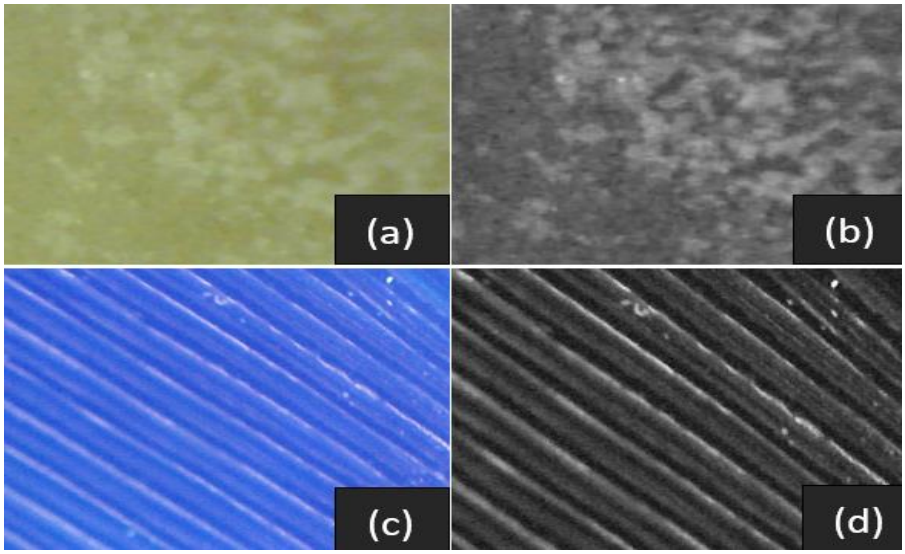

Figure 4: Sample surface in Image processing using Image J (a) SLS original, (b) SLS subtracted background, (c) FDM original, and (b) FDM subtracted background.

2.3 Pressure Drop and Fluid Flow Investigation

Preliminary observations on the printed foams show excessive residues within the porous structure of foam models made of PLA materials. These residues had blocked the pores and cleaning them are difficult due to small pore size, especially for 2 scale model. However, the foam models made of nylon do not have the same issue. The nylon foam also has higher elongation at break percentage as shown in Table 1 which is about 29% higher than PLA. Since the nylon is more likely to deform and not break, the material was preferred to produce the foam models for further investigation on velocity effects in a wind tunnel. The surface roughness of the printed

foam is expected to influence the fluid flow behaviours and pressure drop. Thus, these parameters are investigated in a close loop wind tunnel with air at ambient temperature. The experiment is held in a test section with 0.100m (height) x 0.1m (width) that made from borosilicate glass, aluminium and Bakelite. The ambient air been supplied by a high-pressure blower (AIRSPEC, ARC 629, Power = 3.0 kW) and the air velocity been controlled by an inverter (TECO Inverter F510).

The foam was attached to the bottom side of the test section using a double-sided tape. The foam was also designed to tightly sit between two side walls. The fully filled configuration is created at the test section by installing the porous foams with 0.10 m of height. The samples were positioned in the middle of the test section with only three out of six sides were directly exposed to the air flow. In this study, side 2 was chosen to face the upstream flow due to its lower Ra value to reduce the frictional effects. The air velocity been investigated in two different regions; upstream and downstream as shown in Figure 5 by using a hot-wire anemometer (HT-9830; Accuracy: ±3%+0.2 m/s). The pressure drops have been investigated using pressure sensor where the pressure taps are located at upstream and downstream region with the distance between the taps are 0.16 m. The distance between the foam edge and the measurement location is fixed for all experiments, which is 0.00033 m apart. Different height tests were considered; 0.03, 0.05 and 0.09 m, where the top wall of the test section is the initial point.

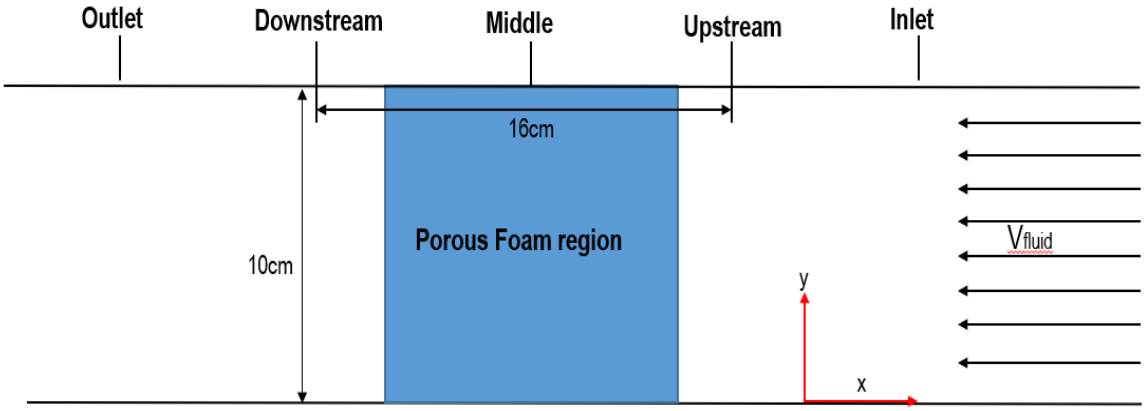

Figure 5: Schematic diagram wind tunnel test section.

3.0 RESULTS AND DISCUSSION

3.1 3D Printed Open-Cell Foam

Figure 6 (a) represents the smallest sample of the 3D printed open-cell foams produced using the SLS technology, where some damaged structures are shown and highlighted in red circles. The smallest foam that is supposed to duplicate the pore size of a real metallic foam has the thinnest and most fragile ligament structure compared to the rest of the upscale samples. As a result, utilizing the above-mentioned procedures and materials, to manufacture 3D printed open-cell foam as small as the original metallic foam, e.g., 10 PPI with 0.00044 m ligament size is impractical due to the limitation of current 3D printing technologies. The ligaments can easily break, and the melted materials could easily fill in the small pores. Meanwhile, different pore sizes are shown in Figure 6 (b) with the upscale factor of 4 and 8. With the larger 3D printed open-cell foam, the

ligament becomes stronger, regardless of the used material. Close inspection shows that the FDM; Flashforge printer with PLA has created more residues (thin strings within the porous structure), as seen in Figure 6 (d), in contrast to the foam produced using SLS. The layering effects could be seen in Figure 6 (d) under a microscope at 60x magnification. Figure 6 (e) from the SLS and cut section shows the nylon powder marks on the interconnected ligaments. Thus, the surface roughness of 3D printed foams should be investigated. Note that the surface roughness could be a significant feature for certain applications where pumping power or contact surface, e.g., an interface between the clear and porous structure of the open-cell foam is a major concern.

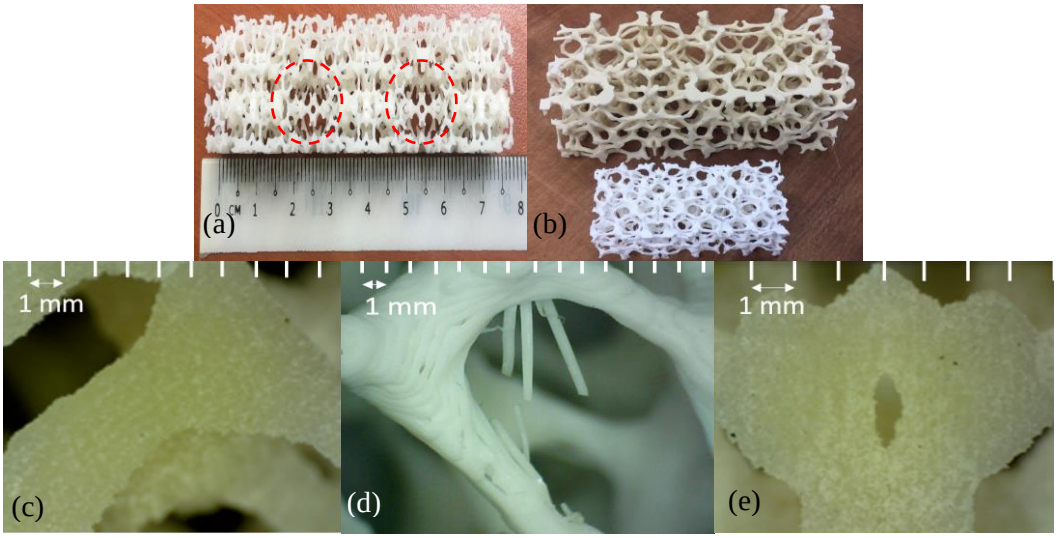

Figure 6: (a) 3D printed foam (0.075m original sample), (b) Enlarged samples with scales of 4 and 8, (c) Interconnected pore-ligament region (d) Residue at FDM structure (e) Cut-section of the foam sample.

3.2 Surface Roughness Evaluation

The analyzed samples are 4 scale samples produced using both SLS and FDM in Figure 7 and Figure 8, respectively. This sample is chosen as it offers high enough surface area, meanwhile the smaller pore sample; 2 scale sample had clogged pores. Since the aim of this study is to introduce a new generation of open-cell foam with very small pores, the smallest scale 3D printed foam with unclogged pores is being investigated. Figure 7 shows the surface plot for 3D printed foams produced using the SLS from the images of three different faces; top, and two sides. The mean calculated surface roughness is 4.553, 5.353, and 4.880 Ra for top, side 1, and side 2, respectively. Thus, there is just a slight difference in surface roughness, regardless of the face sides. The outliers in Figure 7 (b) could be due to imperfect 3D printing quality in that region.

The 3D printed foams produced using the FDM exhibit higher surface roughness as shown in Figure 8. The mean calculated surface roughness for the FDM is about 26.270, 32.133, and 28.395 Ra (top, side 1, and side 2). One of the side surfaces as shown in Figure 8 (b) shows a slightly different pattern as compared to the other two surfaces. Side 1 is the cut-section face (the surface that is used to cover the opened meshes of the CAD drawings), thus providing more arranged peaks compared to the rests.

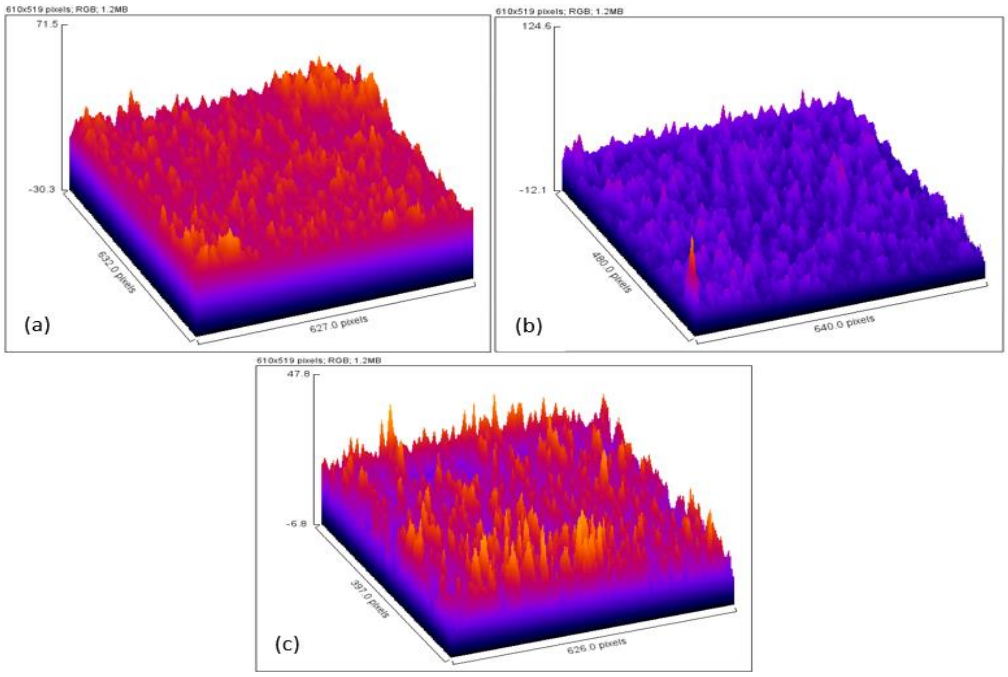

Figure 7: Surface plot for SLS sample; (a) Top, (b) Side 1, and (c) Side 2.

The comparison between these gray values of SLS dan FDM samples is shown in Figure 9, where the values fluctuate within a specific range. However, regardless of the 3D printer types, both sides show similar gray values. Meanwhile, the top side shows the maximum values, with the difference compared to the rest of fluctuated values are about 10 and 20 for SLS and FDM, respectively. The SLS surface in Figure 9 (a) indicates the highest gray value is 20. The randomly scattered powder that has been attached to the ligament surfaces could be the reason for a small difference in the gray values between each face. The profile plot for FDM foam's surfaces is shown in Figure 9 (b). The SLS surface indicates the highest gray value is 93.656 which is also occurred at the top surface. However, the gray values for the FDM sample's faces have significant fluctuation trends as compared to the 3D printed foam from SLS, proving higher surface roughness of 3D printed foam, produced from FDM, even though the same STL files are used. The layering effect (from the printing process) has formed on the external surfaces of foam ligaments, and it could be the main factor that influences the gray values. In an application, when exposing to the fluid flow, this difference is expected to contribute significantly to the values of pressure drop, especially at a higher flow rate.

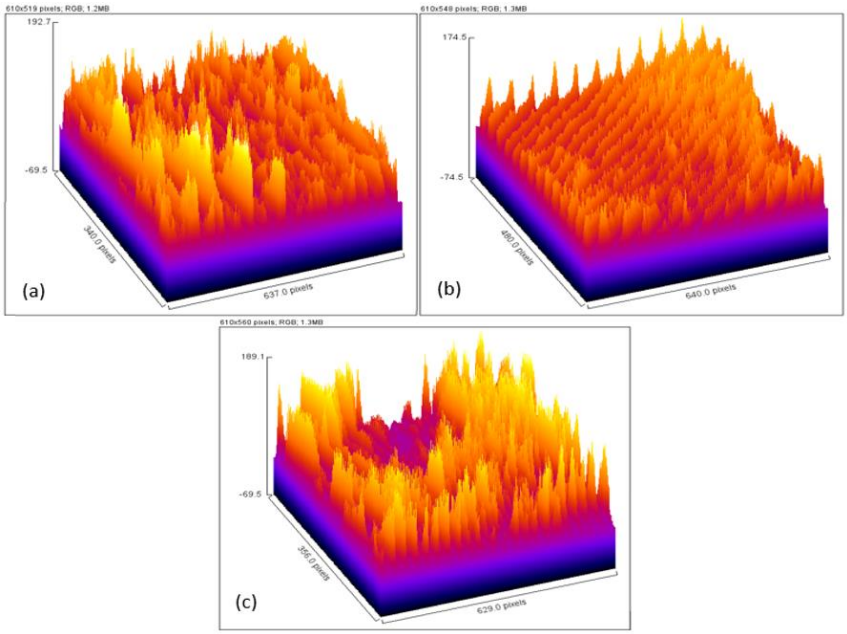

Figure 8: Surface plot for FDM sample (a) Top, (b) Side 1, and (c) Side 2.

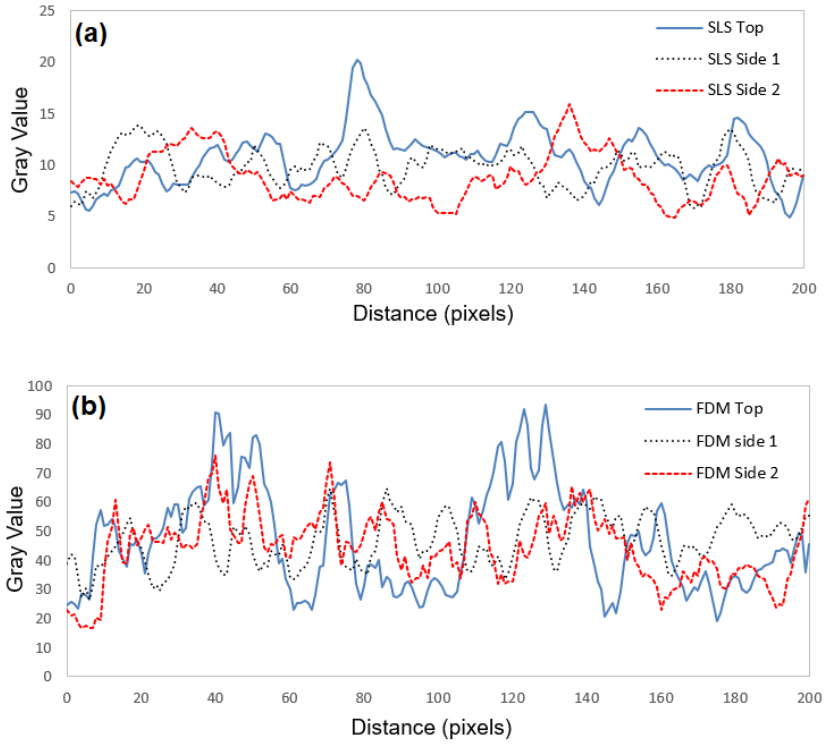

Figure 9: Comparison between faces (a) SLS and (b) FDM.

3.3 Pressure Drop Effect and Velocity Profile

Figure 10 shows the effect of pore size or ligament thickness of the nylon 3D printed foam on the pressure drops. The higher the scale means the pore sizes are larger. The pressure drops of printed foam samples are increasing with the inlet velocity as expected. Using a foam with smaller pores would induce higher pressure drop, which is similar to the trend of original open-cell metal foam subjected to significant foam heights (Shikh Anuar, Ashtiani Abdi, Odabaee, et al., 2018b). Both experiments used the same type of the pressure sensor (Sensirion, 500 Pa; Accuracy: ±3%) and similar size of test section. The foam with a larger pore size, e.g., 8 scale induces smaller pressure drops as expected, since lesser restrictions to the airflow as compared to the samples with 2, 4 and 6 scales. Even though the effect of velocity is higher than the pore sizes, the values are only significant when the inlet velocity through the test section is higher than 3.0 m/s.

Figure 11 shows the effect of pressure drops for nylon 3D printed foams at different height of pressure taps been placed in the test section. Both 3D printed foam with 2 and 8 scale of foam size indicated the pressure drop is lesser at the bottom part of test section (0.03m). The fluid flow characterization is also conducted by investigating the velocity profile inside a small-scale closed loop wind tunnel using a hot-wire anemometer (HT-9830; Accuracy: ±3%+0.2 m/s). Figure 12 shows the velocity profile for 2 and 8 scale pore size samples (a ratio of local velocity over the inlet velocity from the test section entrance) for 2 and 8 scale pore size samples which showed asymmetric pattern at the upstream region, unlike the ideal turbulent velocity profile. With the addition of the foam in the test section, it has changed the flow behaviours in the downstream location, but depending on the pore size, as shown in Figure 12. The 2 scale sample has more significant increase in the downstream velocity as compared to the 8 scale sample, which is expected due to separation flow, right behind the sample. Most of the downstream result showed a wavy pattern where a possibility in turbulence occurrence as the airflow passes through the porous region. The similar pattern for upstream region only occurred for the porous sample with 8 scale of pore size.

Figure 13 shows the comparison the velocity profile of the 3D printed foam with different pore size and inlet velocity at downstream region. The maximum point for 8 scale foams' velocity profile indicated the lowest compared to the other foam. Furthermore, the 8 scale foams tend to have same asymmetric pattern. The 2-scale foam with inlet 1 m/s inlet velocity have the highest value as compared to the other foam which measured from the bottom part of the test section.

CONCLUSION

The complicated structure of open-cell foam has been successfully manufactured using two different additive manufacturing methods; Selective Laser Sintering (SLS) and Fused Deposition Modeling (FDM). The surface roughness from those two samples is studied using the image processing method. Even though the same STL files are used to print out the sample, the surface roughness could be varied significantly, depending on the types of 3D printers and material. However, the pressure drops of 3D printed foams are quite like the metallic ones of the same size and similar experimental setup. Thus, the effects of surface roughness from different manufacturing methods can be overlooked if using the small size of open-cell foam, as used in this study.

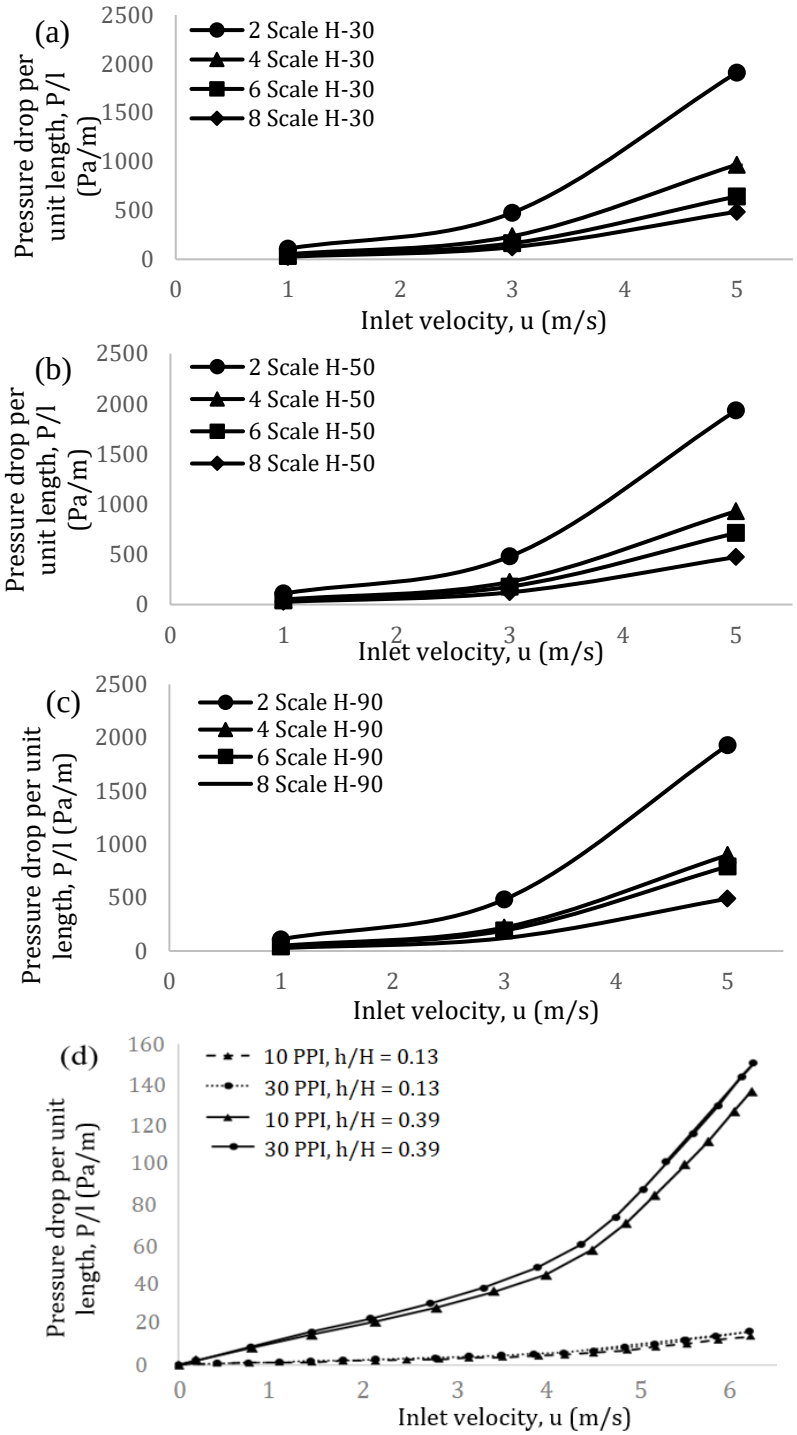

Figure 10: Pressure drops of 3D printed foam at different measuring heighst; (a) 0.03m, (b) 0.05m, and (c) 0.09m and (d)10 PPI and 30 PPI (Shikh Anuar, et al., 2018b).

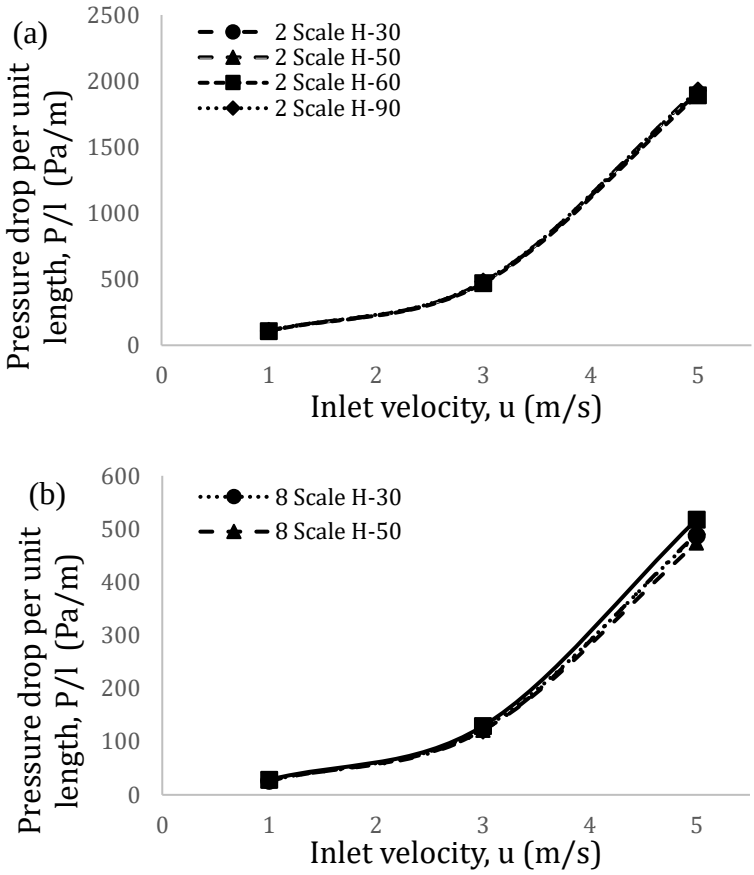

Figure 11: Pressure drops of 3D printed foams with different pore sizes and measuring heights; (a)2 scale, and (b)8 scale.

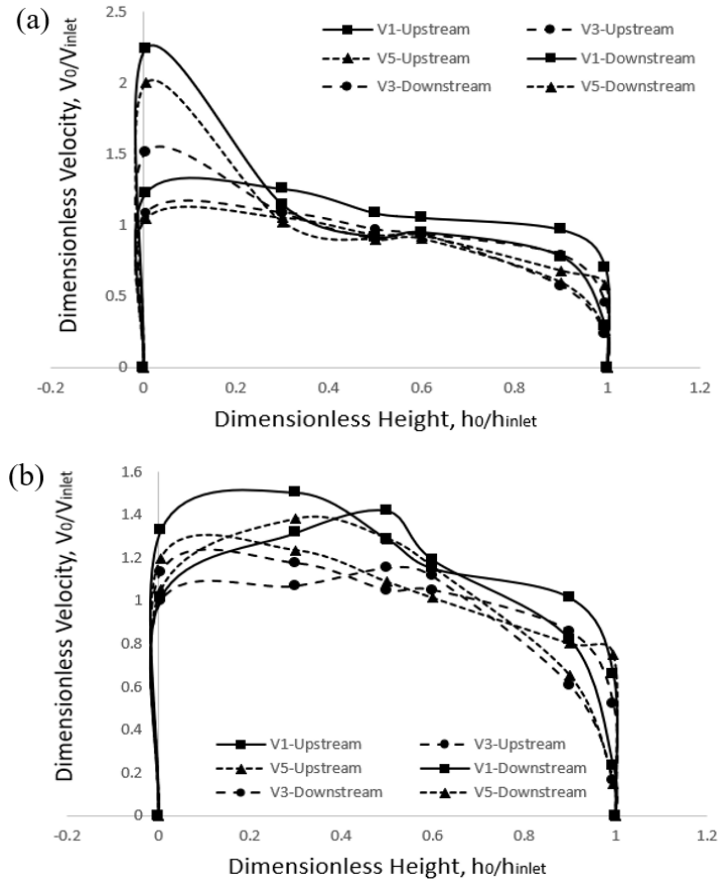

Figure 12: Velocity profiles of 3D printed foam with different pore and ligament sizes; (a)2 scale, and (b)8 scale.

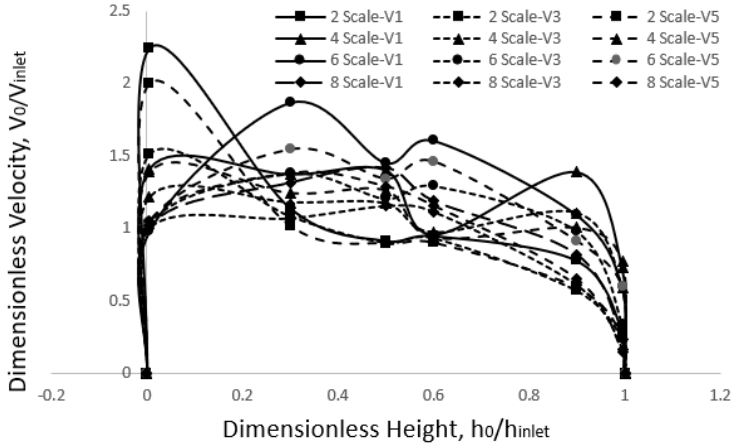

Figure 13: Comparison of 3D printed foams' velocity profile for different pore and ligament sizes at downstream region.

ACKNOWLEDGMENTS

The research was supported by the Ministry of Higher Education Malaysia through Fundamental Research Grant Scheme (FRGS/1/2020/TK0/UTEM/03/2). We also want to thank Universiti Teknikal Malaysia Melaka, which provides the research facilities and Hunan Farsoon High-Tech Co. LTD for the 3D printing material used in this research work.

REFERENCES

Adekanye, S. A., Mahamood, R. M., Akinlabi, E. T., & Owolabi, M. G. (2017). Additive manufacturing: The future of manufacturing: Dodajalna (3D) Tehnologija: Prihodnost Proizvajanja. *Materiali in Tehnologije*, *51*(5), 709–715. https://doi.org/10.17222/mit.2016.261

Ahmed, H. E., Fadhil, O. T., & Salih, W. A. (2019). Heat transfer and fl uid fl ow characteristics of tubular channel partially fi lled with grooved metal foams. *International Communications in Heat and Mass Transfer*, *108*, 104336. https://doi.org/10.1016/j.icheatmasstransfer.2019.104336

Alvandifar, N., Saffar-Avval, M., & Amani, E. (2018). Partially metal foam wrapped tube bundle as a novel generation of air cooled heat exchangers. *International Journal of Heat and Mass Transfer*, *118*, 171–181. https://doi.org/10.1016/j.ijheatmasstransfer.2017.10.104

Banhart, J. (2000). Manufacturing Routes for very low specific. *JOM*, *December*, 22–27.

Farah, S., Anderson, D. G., & Langer, R. (2016). Physical and mechanical properties of PLA, and their functions in widespread applications — A comprehensive review. *Advanced Drug Delivery Reviews*, *107*, 367–392. https://doi.org/10.1016/j.addr.2016.06.012

Herdering, A., Abendroth, M., Gehre, P., Hubálková, J., & Aneziris, C. G. (2019). Additive manufactured polyamide foams with periodic grid as templates for the production of functional coated carbon-bonded alumina foam filters. *Ceramics International*, *45*(1), 153–159. https://doi.org/10.1016/j.ceramint.2018.09.146

Ibrahim, M. B., Veluri, S., Simon, T., & Gedeon, D. (2004). CFD modeling of surface roughness in laminar flow. *Collection of Technical Papers - 2nd International Energy Conversion Engineering Conference*, *1*(August), 556–563. https://doi.org/10.2514/6.2004-5585

Khudiakova, A., Berer, M., Niedermair, S., Plank, B., Truszkiewicz, E., Meier, G., Stepanovsky, H., Wolfahrt, M., Pinter, G., & Lackner, J. (2020). Systematic analysis of the mechanical anisotropy of fibre-reinforced polymer specimens produced by laser sintering. *Additive Manufacturing*, *36*, 101671. https://doi.org/10.1016/j.addma.2020.101671

Kottasamy, A., Samykano, M., Kadirgama, K., Ramasamy, D., Rahman, M. M., & Pandey, A. K. (2021). Optimization of Impact Energy of Copper-Polylactic Acid (Cu-PLA) Composite Using Response Surface Methodology for FDM 3D Printing. *Journal of Advanced Research in Fluid Mechanics and Thermal Sciences*, *84*(1), 78–90. https://doi.org/10.37934/arfmts.84.1.7890

Kumaresan, R., Samykano, M., Kadirgama, K., Ramasamy, D., Keng, N. W., & Pandey, A. K. (2021). 3D Printing Technology for Thermal Application: A Brief Review. *Journal of Advanced Research in Fluid Mechanics and Thermal Sciences*, *83*(2), 84–97. https://doi.org/10.37934/ARFMTS.83.2.8497

Li, B., Wang, J., Liu, R., & Jiang, Y. (2021). Nonlinear fluid flow through three-dimensional rough fracture networks: Insights from 3D-printing, CT-scanning, and high-resolution numerical simulations. *Journal of Rock Mechanics and Geotechnical Engineering*, *13*(5), 1020–1032. https://doi.org/10.1016/j.jrmge.2021.04.007

Liang, L., Wu, X., Ma, N., Du, J., & Liu, M. (2018). The sound absorption properties comparison of

metal foams and flexible cellular materials. *Materials Science Forum*, *933 MSF*, 357–366. https://doi.org/10.4028/www.scientific.net/MSF.933.357

Matheson, K. E., Cross, K. K., Nowell, M. M., & Spear, A. D. (2017). A multiscale comparison of stochastic open-cell aluminum foam produced via conventional and additive-manufacturing routes. *Materials Science and Engineering A*, *707*, 181–192. https://doi.org/10.1016/j.msea.2017.08.102

Norani, M. N. M., Abdullah, M. I. H. C., Abdollah, M. F. Bin, Amiruddin, H., Ramli, F. R., & Tamaldin, N. (2020). Tribological analysis of a 3D-printed internal triangular flip ABS pin during running-in stage. *Jurnal Tribologi*, *27*(July), 42–56.

Norani, M. N. M., Abdullah, M. I. H. C., Abdollah, M. F. Bin, Amiruddin, H., Ramli, F. R., & Tamaldin, N. (2021). Mechanical and tribological properties of fff 3d-printed polymers: A brief review. *Jurnal Tribologi*, *29*(March), 11–30.

Orihuela, M. P., Shikh Anuar, F., Ashtiani Abdi, I., Odabaee, M., & Hooman, K. (2018). Thermohydraulics of a metal foam-filled annulus. *International Journal of Heat and Mass Transfer*, *117*, 95–106. https://doi.org/10.1016/j.ijheatmasstransfer.2017.10.009

Pereira, L., Michna, G. J., & Letcher, T. (2019). *HT2019-3591 The Effects Of 3d Printing Parameters And Surface Roughness ON*. 1–8.

Rabbani, P., Hamzehpour, A., Ashjaee, M., Najafi, M., & Houshfar, E. (2019). Experimental investigation on heat transfer of MgO nanofluid in tubes partially filled with metal foam. *Powder Technology*, *354*, 734–742. https://doi.org/10.1016/j.powtec.2019.06.037

Rocha, T. T. M., de Paula, C. H., Cangussu, V. M., Maia, A. A. T., & de Oliveira, R. N. (2020). Effect of surface roughness on the mass flow rate predictions for adiabatic capillary tubes. *International Journal of Refrigeration*, *118*, 269–278. https://doi.org/10.1016/j.ijrefrig.2020.05.020

Sachlos, E., Czernuszka, J. T., Gogolewski, S., & Dalby, M. (2003). Making tissue engineering scaffolds work. Review on the application ofsolid freeform fabrication technology to the production of tissue engineeringscaffolds. *European Cells and Materials*, *5*, 29–40. https://doi.org/10.22203/ecm.v005a03

Shikh Anuar, F., Ashtiani Abdi, I., & Hooman, K. (2018a). Flow visualization study of partially filled channel with aluminium foam block. *International Journal of Heat and Mass Transfer*, *127*, 1197–1211. https://doi.org/10.1016/j.ijheatmasstransfer.2018.07.047

Shikh Anuar, F., Ashtiani Abdi, I., Odabaee, M., & Hooman, K. (2018b). Experimental study of fluid flow behaviour and pressure drop in channels partially filled with metal foams. *Experimental Thermal and Fluid Science*, *99*(December 2017), 117–128. https://doi.org/10.1016/j.expthermflusci.2018.07.032

Walker, D. C., Caley, W. F., & Brochu, M. (2014). Selective laser sintering of composite copper-tin powders. *Journal of Materials Research*, *29*(17), 1997–2005. https://doi.org/10.1557/jmr.2014.194